12111

Study of the Hyperthermal Proton Bombardment Effects on Self-Assembled Monolayers of Dodecanethiol on Au(111)

Luan Xi,*,† Zhi Zheng,‡,§ Ngai-Sze Lam,‡ Heng-Yong Nie,† Oscar Grizzi,⊥ and Woon-Ming Lau†

Surface Science Western, University of Western Ontario, London, Ontario, Canada, N6A 5B7, Physics Department, Chinese University of Hong Kong, Shatin, Hong Kong, P.R. China, Institute of Surface Micro and Nano Materials, Xuchang University, Xuchang, Henan, 461000, P. R. China, and Centro Atomico Bariloche, 8400 San Carlos de Bariloche, Rio Negro, Argentina

Proton bombardment on self-assembled monolayers (SAMs) of dodecanethiol formed on a gold surface is performed and its effect is studied by scanning tunneling microscope (STM) and time-of-flight secondary ion mass spectrometry (TOF−SIMS). STM gives clear evidence that a relatively uniform layer of organic nanoclusters with different sizes and densities can be created on the surface. Analysis of the mass spectra collected from the SAM samples reveals that large hydrocarbon fragments from the bombarded sample area show higher intensity than those from the virgin area, which is a strong indication that selective C−H bond cleavage and cross-linking are induced by the proton beam bombardment. We demonstrate that the size and density of the clusters can be harnessed by controlling the proton beam energy and fluence. The clusters grow bigger, at the expense of a decreasing number density, with increasing proton energy or fluence.

Introduction

Self-assembled monolayers (SAM) have been recognized as the most promising architecture for device miniaturization. They have incomparable advantages in cost reduction and variability in tuning the surface properties by simply changing the functional group. They are widely used in optical, electrical, mechanical and medical applications. As such, much research has been conducted on their preparation, properties and applications.[1–5] On the other hand, the ease of SAM formation has also facilitated surface science research with molecular precision. In this study, we focus on the ion bombardment effects on SAM, which is a subject that has been studied for many years by several research groups and continues to be an attractive topic under extensive investigation.[6–22] During ion bombardment, an incident ion penetrates to the subsurface region and causes a cascade of collisions. By knocking off the collided target atoms from their equilibrium bonding locations, projectiles in the cascade collisions break bonds even with no thermal energy supply; this may lead to the formation of metastable phases which cannot be synthesized with the conventional chemical reactions driven by thermal energy or catalysts. In most previous studies, cluster ions, heavy ions or ions with a kinetic energy in the order of several hundred electronvolts or more are used.[6–11] Under such relatively violent conditions, the cascade of collisions induced by a single energetic ion arrival may affect more than millions of atoms. The extent of reactivity is obviously too excessive for the modification of a single organic molecular layer on a solid surface such as a SAM. On the other hand, when the energy of the incident species is too low, the change of the surface structure or properties would not be efficient. Indeed it has been found that only minor structure changes occur after exposing SAM to atomic hydrogen with an average energy of 0.07 eV,[13] or 0.4 eV argon and 1.3 eV xenon atoms.[14] Under such mild "bombardment" conditions, the surface reactivity is expected to be dominated by chemistry instead of physical bombardment. In the case of alkanethiolate exposed to 0.11 eV atomic oxygen, oxygen-containing carbon functional group are produced at vacuum/film interface and the monolayer is gradually etched as a result of further reaction of those species with atomic oxygen.[15] In other investigations of the interaction of fluorinated SAM with radicals or polyatomics, complicated processes occur at various sites including atom abstraction, addition and substitution.[16–19] These studies are invaluable for understanding the chemical processes related to SAM stabilities.

It is certainly challenging to control the degree and efficiency of collision-induced reactions with the monolayer, but the reward is high because the fabrication and modification of molecular layers promise many new applications such as molecular-based electronics and biomedical products. In this context, the ion energy must be reduced to confine the bombardment induced chemical changes close to the surface but this alone does not meet the challenge. The ideal solution would comprise leveraging the high chemical reactivity induced by coupling the ion kinetic energy and the activation derived from the cascade collisions to desirable chemical effects and, at the same time, finding means to control chemical selectivity for promoting the desirable chemical reaction with no undesirable side-reactions.

A new ion collision-induced reaction method was recently introduced by Lau and co-workers to demonstrate the feasibility of such an ideal solution.[23,24] In this method, the lightest ion species, the proton, with a hyperthermal energy of about 2−50 eV is used to bombard organic precursor molecules condensed on a substrate surface. A large volume of experimental results[23,24] have demonstrated that the light projectiles can transfer their kinetic energy effectively to H atoms in the precursors but the energy transfer is ineffective for other target

* To whom correspondence should be addressed. E-mail: lxi3@uwo.ca.
† The University of Western Ontario.
‡ The Chinese University of Hong Kong.
§ Xuchang University.
⊥ Centro Atomico Bariloche.
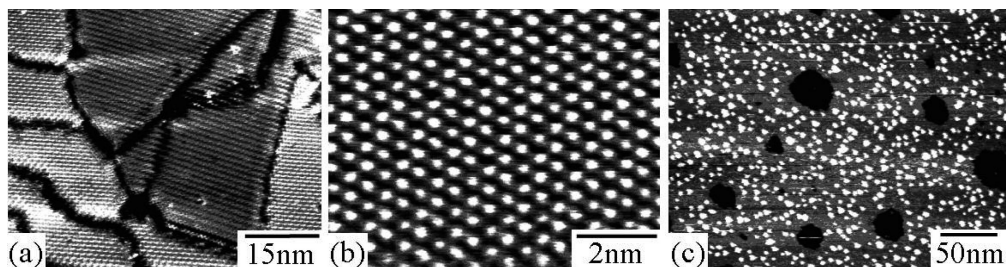
Figure 1. STM images of C12 SAMs prepared on an Au(111) substrate: (a and b) before any bombardment; (c) after the bombardment by a 3 eV H$^+$ beam with a fluence of 3×10^{15} ions/cm^2.

atoms. The experimental results are supported by the theoretical prediction derived from the simple binary collision approximation. This leads to the realization of a collision-induced dissociation process in which C−H bonds are preferentially cleaved, and other bonds are intact under the optimal experimental conditions. When the resultant carbon radicals recombine, the precursors are cross-linked to a polymeric molecular layer with the chemistry governed by that of the precursors, and the mechanical properties governed by the degree of cross-linking.

In the context of reacting SAMs with hydrogen, several studies with atomic hydrogen are also known.[20–22] For example, Gorham, et al., studied the influence of chain length on the modification of SAM layers by exposure to atomic hydrogen.[20] This group found that the loss of sulfur exhibits first order kinetics with the rate constant decreasing with increasing alkyl chain length. Based on this observation, the group proposed that for dodecanethiol (C12) and nonanethiol (C9) SAM, the modification by atomic hydrogen is dominated by desorption of intact chains due to the reaction of the atomic hydrogen and the head sulfur group. For octadecanethiol (C18) and hexadecanethiol (C16) SAM, the long chain length favors hydrogen abstraction from the carbon chain. The resultant carbon radical formation leads to cross-linking of the SAM molecules. This reaction mechanism via hydrogen abstraction is also supported by the previous observation[21] of hydrogen/deuterium exchange when an SAM grown on a silicon wafer was exposed to atomic hydrogen/deuterium. Another investigation of the modification of fluorinated SAMs by atomic hydrogen also shows that the hydrogen abstraction can lead to the desorption of species that contain the fluorocarbon.[22]

The present article reports on the results that when a beam of protons with precisely controlled energy and fluence is used to bombard a C12 SAM on Au(111), a relatively uniform layer of nanoclusters can be produced by appropriate collision-induced dissociation of the SAMs to initiate the desirable cross-linking reactions. The reaction strategy allows the control on the size and size-distribution of nanoclusters comprising cross-linked alkanethiols, which is confirmed by scanning tunneling microscopy. The cross-linking reaction is further confirmed by using time-of-flight secondary ion mass spectrometry (TOF−SIMS) to track the presence of molecular species larger than the C12 precursor.

Experimental Section

The Au(111) substrates were purchased from the Molecular Imaging Corporation and subjected to hydrogen flame annealing before use. After the treatment, the formation of the well-known triangular-shaped terraces and $\sqrt{3} \times 23$ herringbone surface structure were evident.

Dodecanethiol (C12) was purchased from the Sigma-Aldrich Corporation and used without further purification. The self-

assembling of the thiols was carried out by immersing an Au(111) substrate into a 1 mM ethanolic solution of C12 for a few minutes. Then the sample was rinsed carefully with pure ethanol and dried by a nitrogen gas flow.

The hyperthermal proton bombardment was performed with a home-built mass-separated low energy ion beam system.[26] The STM experiments were performed using an Omicron VT SPM system. TOF−SIMS investigations were carried out using an ION-TOF TOF−SIMS IV system with a bismuth liquid metal ion source. The 25 keV primary ion (Bi$^+$) beam was pulsed, with a 1.5 μm spot size and a target current of 2 pA. To achieve the best mass resolution, we adopted the high current bunched mode.

Results and Discussion

After growing the C12 SAM on Au in solution, we further annealed the C12 SAM in UHV at 80 °C for 2 h to improve the ordering. The STM images of C12/Au after annealing are shown in Figure 1, (a) and (b). The high resolution image of the well-known standing-up $\sqrt{3} \times \sqrt{3}$ phase is clearly displayed in Figure 1 (b). This confirms that the virgin C12/Au prior to any ion bombardment is indeed a good SAM model system. The bombardment is expected to cause some changes of the surface structure of the SAM, which may need to be viewed in a spatial field larger than the field of 8.3 nm × 6.5 nm in Figure 1 (b). Hence, the STM image of a field of 64 nm × 52 nm is shown in Figure 1 (a). In this field of view, atomically flat domains having the standing-up $\sqrt{3} \times \sqrt{3}$ phase are seen. The commonly observed Au vacancy islands (VI) induced by molecular assembling are present on the surface, but not shown in the specific areas imaged in Figure 1, (a) and (b).

After bombardment by 3 eV H$^+$ with a fluence of 3×10^{15} ions/cm^2, the ordered SAM structure is modified to a dispersed distribution of nanoclusters on the surface as shown in Figure 1 (c). The apparent size of the nanocluster is about 5 nm, with a narrow size variation. The nanoclusters are quite uniformly spaced. To explain the mechanism with which the standing-up $\sqrt{3} \times \sqrt{3}$ phase of C12 molecules is converted to nanoclusters of 5 nm, we first note that when the proton projectile approaches to ~0.5 nm from the top of the SAM/Au surface, electrons below the Fermi level of the surface (work function of 4−5 eV) will tunnel to the empty electronic state of the proton (13.6 eV). The neutralization probability is very high. So prior to any other changes, the proton projectile is converted to a hyperthermal hydrogen atom with a kinetic energy of 3 eV. As discussed earlier,[25] under the conventional hard-sphere binary collision model, the energy transfer from a hydrogen projectile is most effective to the hydrogen atom on the target. Hence, the energy transferred to C and S is at most 0.85 and 0.35 eV respectively, which is below the bond energy of C−C and S−C and the dissociation energy barriers of them. In contrast, the energy that a hydrogen atom receives can be as much as 3 eV,

TABLE 1: Relative Intensity of Selected Secondary Ion Species of the Bombarded Area Ratioed to Those from the Virgin C12/Au (Sample 1, 2 eV, 5×10^{15} ions/cm^2; Sample 2, 3 eV, 5×10^{14} ions/cm^2)

negative ions	mass	sample 1	sample 2	positive ions	mass	sample 1	sample 2
Au	197.0	1.6	1.1	Au	197.0	0.2	0.7
AuS_2	260.9	1.6	1.2	AuS_2	260.9	0.3	0.5
HS_2Au_2	458.9	1.3	1.1	HS_2Au_2	458.9	0.5	0.7
$C_{13}H_8$	164.1	2.3	2.2	$C_{15}H_{26}$	206.2	48.5	2.3
$C_{14}H_{10}$	178.1	5.7	2.0	$C_{17}H_{36}S$	272.3	4.3	2.5
$C_{15}H_{13}S$	225.1	8.1	2.1	$C_{23}H_{20}S_2$	360.1	14.9	1.2
$C_{15}H_3S_2$	247.0	2.4	1.9	$C_{25}H_{26}S_2$	390.2	15.8	1.2
$C_{19}H_{19}$	247.1	9.8	2.3	$C_{36}H_{53}$	485.5	4.4	1.8
$C_{16}H_{25}SO$	265.1	5.4	2.2	$C_{38}H_{53}$	509.5	4.0	2.1
$C_{23}H_3$	279.0	14.4	1.8	$C_{38}H_{57}$	513.5	6.2	1.8
$C_{15}H_{17}S_3$	293.0	7.6	2.2	$C_{39}H_{55}$	523.5	3.2	1.6
$C_{23}H_{19}$	295.1	8.7	3.7	$C_{39}H_{59}$	527.5	5.7	2.0
$C_{16}H_{25}S_2O$	297.1	7.2	2.3	$C_{40}H_{59}$	539.5	4.9	1.7
$C_{17}H_{37}S_2O$	321.2	9.4	1.7	$C_{40}H_{61}$	541.5	5.9	2.8
$C_{19}H_{41}S_2O$	349.2	9.5	2.4	$C_{39}H_{67}S_3$	631.5	5.1	2.9
$C_{22}H_{35}S_2$	363.2	3.8	2.1	$C_{40}H_{67}S_3$	643.5	5.7	2.3
$C_{21}H_{45}S_2O$	377.3	6.8	2.7	$C_{40}H_{69}S_3$	645.5	8.8	2.3
$C_{25}H_{34}S_2$	398.2	10.4	2.4	$C_{41}H_{69}S_3$	657.5	5.8	2.2
$C_{23}H_{49}S_2O$	405.3	4.9	3.4	$C_{41}H_{71}S_3$	659.5	7.1	2.6
$C_{28}H_{49}SO$	433.3	5.2	4.1	$C_{42}H_{71}S_3$	671.5	6.7	2.3
$C_{25}H_{53}S_3O$	465.3	9.8	3.6	$C_{42}H_{73}S_3$	673.6	10.8	2.3
$C_{30}H_{21}S_3$	477.1	19.1	3.1	$C_{42}H_{75}S_3$	675.6	8.1	2.4
$C_{26}H_{55}S_3O$	479.3	18.3	4.3	$C_{43}H_{73}S_3$	685.5	6.2	1.9
$C_{27}H_{53}S_3O$	489.3	13.2	6.0	$C_{43}H_{75}S_3$	687.6	8.6	2.1
$C_{27}H_{55}S_3O$	491.3	34.8	11.2	$C_{44}H_{75}S_3$	699.5	5.9	2.6
$C_{28}H_{57}S_3O$	505.3	11.1	11.3	$C_{44}H_{77}S_3$	701.6	9.3	1.8
[a]		9.9	3.5	[a]		9.0	2.1

[a] Mean value of the intensity ratios of ion species listed in the table excluding the first 3 Au related ones.
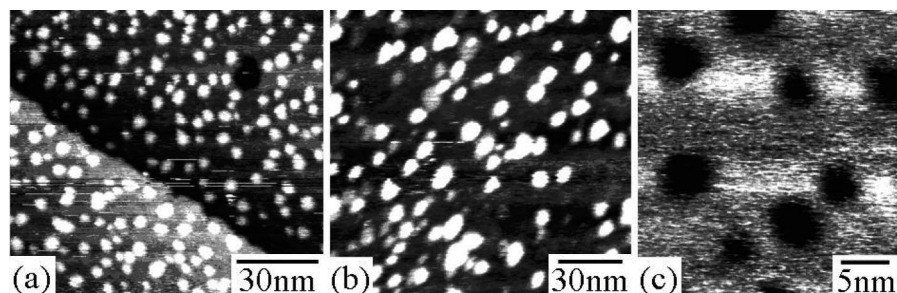

Figure 2. STM images of C12/Au subjected to H$^+$ bombardment of primary beam energy and fluence at (a) 2 eV, 5×10^{15} ions/cm^2, (b) 3 eV, 5×10^{15} ions/cm^2, and (c) 6 eV, 2×10^{15} ions/cm^2.
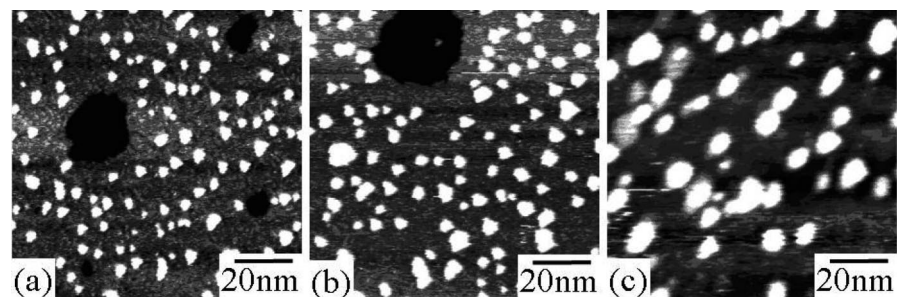
Figure 3. STM images of C12/Au subjected to 3 eV H$^+$ bombardment, the H$^+$ dosage is (a) 2×10^{15} ions/cm^2, (b) 3×10^{15} ions/cm^2, and (c) 5 $\times 10^{15}$ ions/cm^2.

which is enough to cleave C−H bonds as demonstrated experimentally by Lau and co-workers.[24] The reactivity of C−H bond cleavage with this unusual means has also been found[24] to be much higher than that of simple hydrogen abstraction with thermal atomic hydrogen. When the C−H bonds of a C12 molecule are cleaved, a C12 molecule can then be changed to a C12 molecule having a carbon radical. The dissipation of the bombardment energy to atoms/molecules near the impact site may also enhance the surface diffusion of the C12 radical. When

two C12 radicals meet, they can recombine by forming a C−C cross-link. The effect shortens the intermolecular separation and produces great stress between molecules, which weakens the S−Au bonds. This, with the dissipation of bombardment energy to local transient thermal energy may lead to the cleavage of some S−Au bonds, desorption of some C12 or cross-linked molecules, and surface diffusion of the residual molecules. The original standing-up $\sqrt{3} \times \sqrt{3}$ phase is thus lost and replaced by a distribution of nanoclusters. Each nanocluster is an

aggregation of cross-linked C12 molecules with one or more S−Au bonds. Unreacted C12 molecules may be trapped in some of these nanoclusters. Some of the cross-linked molecules may have multiple C12 base units, and the probability of this will increase with the degree of cross-linking which can be raised by either increasing the fluence or energy of the incident projectiles.[24] Although the partial conversion of the impact energy to a transient thermal energy at the impact site is likely a driving force of surface diffusion, raising the substrate temperature by the bombardment is below the detection limit by direct temperature measurements with a thermocouple and with an infrared pyrometer. In a relevant set of experiments with the same bombardment conditions, we bombard a layer of physiosorbed $CH_3(CH_2)_{30}CH_3$ on a silicon wafer and observe no desorption. In addition, we observe that the nanoclusters formed in this work desorb quickly from the surface when the substrate temperature is raised by resistive heating to 80 °C. Hence, a rise of substrate temperature induced by bombardment should not be a significant attribute driving the observed nanocluster formation.

Fogarty and Kandel have also studied the structure changes of octanethiol SAM after repeated collisions with 0.4 eV argon and 1.3 eV xenon atoms.[14] They found that the closely packed monolayers remain largely unchanged, and that structural changes happen near defects, domain boundaries and disorder regions of the SAM. By using the simple hard-sphere binary collision model again, one finds that the maximum energy transfer from Ar to H is 9.5%, Ar to C 71%, Ar to S 99%, Xe to H 3%, Xe to C 31%, and Xe to S 63%. Hence, in the bombardment conditions of Fogarty and Kandel, kinematic energy transfer is most effective for collisions with the S atoms. In the SAM adlayer, S atoms are more accessible to the incoming projectiles at the defect sites and domain boundaries. We believe that these two factors of energy transfer and "target" accessibility lead to the observed results of Fogarty and Kandel. In contrast to this, Kautz, et al., found that when a SAM is exposed to hydrogen atoms, structure changes also occur in the close packed region.[13] We believe that these changes are driven by hydrogen abstraction which leads to the creation of carbon radicals and subsequent cross-linking. The reactivity in this case is much lower than our case of proton bombardment.[25] Indeed, the results of Kautz, et al., indicate[13] no obvious structural changes even when the fluence of hydrogen atoms reaches $10^{17}/cm^2$. In comparison, the structural changes shown in Figure 1 (c) are induced by 3 eV H^+ with a fluence of $3 \times 10^{15}/cm^2$.

To study the chain length effects, we have also performed proton bombardment on ethanethiol (C2) SAM. When the C2 SAM is subjected to 2 eV, $5 \times 10^{15}/cm^2$ H^+ bombardment, the ordered SAM domains disappear and some cluster protrusions emerge. In comparison to C12 bombarded at the same condition, the number density of the clusters is much smaller for the case of C2. The higher desorption rate is in consistent with the results of Gorham, et al.[20] On the other hand, the observation of nanocluster formation in the case of C2 indicates that cross-linking happens to short molecules too. The higher desorption rate relative to that of C12 can be attributed to the reduced van der Waals force between the hydrocarbon chains as the chain length gets shorter. The increase in accessibility of the sulfur headgroup to the hyperthermal hydrogen also enhances the probability of S−Au bond cleavage.

The bombardment effects on the C12/Au SAM model are further examined by TOF−SIMS to verify the cross-linking hypothesis (the raw mass spectra are available in the Supporting Information). In this comparison, the TOF−SIMS experiments on the bombarded and unbombarded areas are carried out under the same conditions. A comparison of the mass spectra shows that the unbombarded sample area only contains a few peaks that have higher intensities than those of the bombarded one in the positive spectra. Some of these peaks are Au^+, S_2Au^+, S_3Au^+, $H_2S_3Au^+$, $HS_2Au_2^+$, and $C_{12}H_{25}SAu_2^+$. However in the negative spectra, the counter peaks such as Au^-, SAu^-, S_2Au^-, HS_2Au^-, Au_2^-, SAu_2^-, $S_2Au_2^-$, $HS_2Au_2^-$, and $C_{12}H_{24}SAu^-$ all have higher intensity in the bombarded area compared to the unbombarded one. These peaks are all associated with the substrate and because of the different ratios in positive and negative spectra, no direct information about the relative density of the S−Au bonds before and after bombardment can be readily derived.

Despite the fact that the molecular coverage on the Au(111) surface is significantly reduced after bombardment, we find that in both the negative and positive spectra, the intensity of many of the high mass species, in the form of C_xH_y, $C_xH_yS_2$, $C_xH_yS_2O$, $C_xH_yS_3$, $C_xH_yS_3O$, of the bombarded area are consistently and significantly higher than those of the virgin C12/Au. The results are summarized in Table 1. The results clearly show the evidence of the presence of larger molecules on the bombarded areas, this verifies the cross-linking hypothesis. As shown later in this article, we have compared the effects of varying the energy (2, 3, and 6 eV) and fluence of the bombardment ($10^{14}–10^{16}/cm^2$). From this work and the related prior work of Lau and co-workers,[24] we know that bombardment at a relative low impact energy of 2−3 eV and a low fluence of about 1×10^{15} ions/cm² can readily lead to a measurable degree of cross-linking (typically measured by the amounts of molecules in a film of $C_{32}H_{66}$ of ~10 nm being converted from soluble in hexane before bombardment to insoluble to hexane after bombardment[24]). The results in Table 1 indeed confirm that the cross-linking effect is also measurable with TOF−SIMS for the very mild condition of 3 eV and 5×10^{14} ions/cm². At this low fluence, the cumulative proton arrivals amount to about one monolayer equivalent. Hence, the cross-linking efficiency is certainly not low. When the fluence is increased to 5×10^{15} ions/cm², the bombardment at 2 eV yields a much higher degree of cross-linking as indicated by the mean value of the intensity ratios of selected high mass species at the bottom of Table 1. Therefore, the cross-linking efficiency at 2 eV is still very high.

An interesting feature in the observed nanocluster formation is that the clusters are relatively uniform both in size and distribution as shown in Figure 1 (c) suggesting that their formation is governed by certain factors balancing the diffusion and cross-linking of the modified thiol molecules. It is conceivable that the proton beam energy and fluence play important roles in the observed nanocluster formation. To prove this hypothesis, we use STM to track the effects of energy and fluence on nanocluster formation.

The effects of proton energy at a constant fluence are illustrated in Figure 2. Increasing proton energy from 2 to 3 eV gives fewer but larger clusters, which indicates more cross-linking and longer diffusion distance. The typical respective cluster diameters for 2 and 3 eV bombardment are 5 nm and 7−8 nm. When the proton energy is increased, the energy transferred to hydrogen atoms on C12 is increased, which increases the probability of C−H bond cleavage. The diffusion distance is increased as a result of the conversion of some of the bombardment energy to a transient rise of the thermal energy near the impact site. For proton energy of 6 eV, thiol molecules are effectively desorbed.

As shown in Figure 3, the size of the nanoclusters grows with increasing H$^+$ fluence at a constant energy of 3 eV. The respective average diameters of nanoclusters are about 4, 5, and 7−8 nm for the fluences of 2×10^{15}, 3×10^{15}, and 5×10^{15} ions/cm^2. As the fluence increases, the number of C−H bond cleavage increases. Some C−H bonds of a small cluster are thus broken, which leads to more cross-links in the cluster but may also leave some carbon radicals on the "surface" of the cluster. The diffusion of some of these small clusters will lead to the meeting of clusters with carbon radicals on their "surfaces". This drives the coalescence of the nanoclusters. If the cluster adsorption energy is reduced too much due to the induced bond strain and weakening of Au−S bonds at the cluster−Au interface, the cluster may be desorbed. Hence, increasing fluence may decrease the total amount of adsorbate mass on the surface too. For an extremely high fluence, all SAM molecules are driven off the surface.

Conclusions

We have used STM and TOF−SIMS to reveal morphological and chemical evidence on cross-linking alkanethiol molecules from their SAMs on Au(111) surface into nanoclusters via bombardment by hyperthermal protons with an energy of 2−6 eV. By properly controlling the incident proton beam energy and fluence, we can create a uniformly distributed alkanethiol molecular nanoclusters on the gold surface. The size of the clusters increases and their number density decreases with increasing proton beam energy or fluence.

Supporting Information Available: Figures showing TOF−SIMS spectra of two sets of samples partly subjected to proton beam bombardment. This material is available free of charge via the Internet at http://pubs.acs.org.

References and Notes

(1) Ulman, A. *Chem. Rev.* **1996**, *96*, 1533.
(2) Sandhyarani, N.; Pradeep, T. *Int. Rev. Phys. Chem.* **2003**, *22*, 221.
(3) Wink, T.; van Zuilen, S. J.; Bult, A.; van Bennekom, W. P. *Analyst* **1997**, *122*, R43.
(4) Schreiber, F. *J. Phys.: Condens. Matter* **2004**, *16*, R881.
(5) Ulman, A. *An Introduction to ultrathin organic films: from Langmuir-Blodgett to self-assembly*; Academic Press: Boston, MA, 1991.
(6) Wong, S. C. C.; Lockyer, N. P.; Vickerman, J. C. *Surf. Interface Anal.* **2005**, *37*, 721.
(7) Chenakin, S. P.; Heinz, B.; Morgner, H. *Surf. Sci.* **1999**, *421*, 337.
(8) Chenakin, S. P.; Heinz, B.; Morgner, H. *Surf. Sci.* **1999**, *436*, 131.
(9) Harris, R. D.; Baker, W. S.; Van Stipdonk, M. J.; Crooks, R. M.; Schweikert, E. A. *Rapid Commun. Mass Spectrom.* **1999**, *13*, 1374.
(10) Riederer, D. E.; Chatterjee, R.; Rosencrance, S. W.; Postawa, Z.; Dunbar, T. D.; Allara, D. L.; Winograd, N. *J. Am. Chem. Soc.* **1997**, *119*, 8089.
(11) Varghese, B.; Dorothy, A.; Pradeep, T. *Int. J. Mass Spectrom. Ion Processes* **1996**, *155*, 69.
(12) Liu, K. S. S.; Vickerman, J. C.; Garrison, B. J. *Radiat. Eff. Defects Solids* **1997**, *142*, 205.
(13) Kautz, N. A.; Fogarty, D. P.; Kandel, S. A. *Surf. Sci.* **2007**, *601*, L86.
(14) Fogarty, D. P.; Kandel, S. A. *J. Chem. Phys.* **2006**, *124*, 111101.
(15) Wagner, A. J.; Wolfe, G. M.; Fairbrother, D. H. *J. Chem. Phys.* **2004**, *120*, 3799.
(16) Shen, J. W.; Grill, V.; Evans, C.; Cooks, R. G. *J. Mass Spectrom.* **1999**, *34*, 354.
(17) Shen, J.; Grill, V.; Cooks, R. G. *J. Am. Chem. Soc.* **1998**, *120*, 4254.
(18) Luo, H.; Miller, S. A.; Cooks, R. G.; Pachuta, S. J. *Int. J. Mass Spectrom.* **1998**, *174*, 193.
(19) Burroughs, J. A.; Hanley, L. *Anal. Chem.* **1994**, *66*, 3644.
(20) Gorham, J.; Smith, B.; Fairbrother, D. H. *J. Phys. Chem. C* **2007**, *111*, 374.
(21) Kluth, G. J.; Sung, M. M.; Maboudian, R. *Langmuir* **1997**, *13*, 6491.
(22) Gorham, J. M.; Stover, A. K.; Fairbrother, D. H. *J. Phys. Chem. C* **2007**, *111*, 18663.
(23) Zheng, Z.; Kwok, W. M.; Lau, W. M. *Chem. Commun.* **2006**, *29*, 3122.
(24) Zheng, Z.; Xu, X. D.; Fan, X. L.; Lau, W. M.; Kwok, R. W. M. *J. Am. Chem. Soc.* **2004**, *126*, 12336.
(25) Xi, L.; Zheng, Z.; Lam, N. S.; Grizzi, O.; Lau, W. M. *Appl. Surf. Sci.* **2007**, *254*, 113.
(26) Lau, W. M.; Feng, X.; Bello, I.; Sant, S.; Foo, K. K.; Lawson, R. P. W. *Nucl. Instrum. Methods Phys. Res., Sect. B* **1991**, *59*, 316.

JP710802R